Development of Particulate Matter Monitors based on Light Scattering Method

Junjie Liu (0000-0002-4014-9841)[1]*, Laihua Yu (0009-0008-4537-1020)[2], Jing Ye (0009-0003-1361-5717)[3], Zhihuang Huang (0009-0009-5583-6976)[3], Jiazhen Lu (0009-0007-6919-4519)[3], Yue Liu (0009-0003-9841-9167)[1]*
[1]Environmental Metrology Centerr, National Institute of Metrology, Beijing, 100013, China; E-mail: liujj@nim.ac.cn; liu-yue@nim.ac.cn
[2] Aviation Industry (Xinxiang) Metrology and Test Science Technology Co., Ltd, Xinxiang 453019, Henan province, China; zybzzybylh@163.com
[3] College of Chemical Engineering and Technology, Taiyuan University of Technology, Taiyuan 030010, Shanxi province China; yejing147@outlook.com; 2682817016@qq.com
[4] Fujian Metrology Institute, Fuzhou 350003, Fujian province, China; hanmenyeye@163.com
Correspondence: liu JJ, liujj@nim.ac.cn; +86 10 64524974; liu Y, liu-yue@nim.ac.cn; +86 10 64525036

$PM_{2.5}$ and PM_{10} measurement technique based on light scattering usually exhibit inaccurate measurement results in their applications. For improving the reliability of this method for $PM_{2.5}$ and PM_{10} measurement, systematic research on the structure optimization of single particle light scattering sensors (SPLSS), calibration of SPLSS, and $PM_{2.5}/PM_{10}$ monitor development are carried out. Frist, by simulating and optimizing light scattering parameters, light scattering signals varied monotonically with particle size could be obtained, and thereby capability of accurate size-identifying can be established. Then, by developing threshold comparison circuit and calibration device, particle size channel of SPLSS or monitor could be divided, and particle counting efficiency could be corrected. Finally, by obtaining empirical values of parameters, i.e., heating temperature, particle density, involved in the developed dynamic heating system and PN-PM algorithm, interference of humidity and particle characteristics can be effectively eliminated, thus particle mass concentration (PM) could be calculated according to particle number concentration (PN) in each channel. The results show that the developed monitor has good accuracy by comparing it in atmospheric air with reference methods of $PM_{2.5}/PM_{10}$.

Keywords: $PM_{2.5}$, PM_{10}, mass concentration, sensor, calibration

1 Introduction

The rapid industrialization and urbanization process has greatly improved our life level, while also bringing serious air pollution, such as inhalable particulate matter (PM_{10}) and fine particulate matter ($PM_{2.5}$). The air pollution caused by $PM_{2.5}/PM_{10}$ not only greatly harm to human health, but also seriously hinders economic development [1-3]. Faced with the severe environmental pollution and governance needs, $PM_{2.5}/PM_{10}$ daily monitoring have been carried out in many countries, e.g., in China, not only a huge monitoring network been established, but also systematic technical regulations for measurement methods or monitors have been completed [4,5].

Currently, four kinds of $PM_{2.5}/PM_{10}$ measurement methods are available [6-11], i.e., tapered element oscillating microbalance (TEOM), Beta gauge, gravimetric method, and light scattering. The gravimetric method is based on filter membrane weighing, which can make mass concentration of particulate matter trace to SI unit, therefore, it has already been considered as a reference method for $PM_{2.5}/PM_{10}$ [7]. However, to make electronic balance employed in method can output accurate results, it is necessary to load enough particulate matter on the filter membrane, so it is actually a time-consumed method and cannot output real-time results. As continuous automatic methods for $PM_{2.5}$ and PM_{10}, TEOM method and Beta gauge method can output measurement results per less than 1hour with high accuracy and sensitivity [7], but both methods are relatively expensive and impactors with nominal 50% cut-points of 2.5µm and 10µm are required to obtain aerosol samples meet the definition according to aerodynamic principle.

Compared with the above methods, light scattering method for $PM_{2.5}/PM_{10}$ has the advantages of low-cost, outputting real-time results with interval of seconds-level, etc. By using monitors or sensors based on this low-cost technology, high-density monitoring network in specific areas, such as industrial zone or residential community, could be established, and real-time $PM_{2.5}/PM_{10}$ monitoring date and emission behavior within regions can be detected in time [10,11]. However, in light scattering measurement technology, due to significant effect of particle characteristics (density, refractive index, shape factor, particle size distribution, etc.) and instrument

characteristics (scattering angle, scattering solid angle, etc.), measurement results by light scattering method are unsatisfactory in many cases [12-21]. For effectively improve the accuracy and reliability of $PM_{2.5}/PM_{10}$ monitor based on this method, in this paper, a $PM_{2.5}/PM_{10}$ monitor based on the single particle light scattering was developed, where, the sensor's structure was optimized to ensure well-correspondence between output signal and particle size, sensor's particle size channels and count efficiency were calibrated to make the output signal (particle number concentration, PN) in each channel more reliable, the empirical values of parameters, i.e., heating temperature, particle density, involved in the developed dynamic heating system and PN-PM algorithm, were achieved.

2 Materials and Methods

2.1 Design of $PM_{2.5}/PM_{10}$ monitor

2.1.1 Simulation and theoretical analysis of light scattering

Mie scattering is the theoretical basis of light scattering method for airborne particle size and further concentration measurement [2], where light scattering flux (F), derived from single equivalent spherical particle in the light scattering zone, is an important output signal that reflects the characteristics of particles. The F can be represented by equation 1, which is closely relate to such parameters as $D, \theta, \Delta\Omega, \lambda$ and m. Among those parameters, λ, θ and $\Delta\Omega$ are associated with sensors' structure.

$$F(D, \theta, \Delta\Omega, \lambda, m) = I_0 \frac{\lambda^2}{4\pi^2} \iint_{\Delta\Omega} i(\theta, \Phi, \alpha, m) \sin\theta \, d\theta \, d\Phi \tag{1}$$

Where:

i…The particle's scattering function in the space,

D…The particle size,

θ…The scattering angle,

$\Delta\Omega$…Solid angle of collected scattering light,

I_0, λ and Φ …The intensity, wavelength and polarization angle of laser,

m…The relative refractive index of particles,

α …Parameter related to particle size, which is equal to $(\pi D)/\lambda$.

Making light scattering signals varied monotonically with particle size is critical to effectively identify and measure airborne particles with different sizes according to F. For a sensor configured with a certain laser source, F is mainly dependent on θ and $\Delta\Omega$ if the measurand is not considered. Here, $F\sim D$ relationship with different θ and $\Delta\Omega$ values was simulated using MTALAB software by assuming the particle's relative refractive index (m=1.688), laser wavelength (λ=650 nm). In the condition of setting solid angle of collected scattering light ($\Delta\Omega$) to 30 °, the simulated $F\sim D$ characteristic curves at different scattering angle (θ=30 °, 45 °, 60 °, 75 °, and 90 ° respectively) could be obtained as shown in Fig. 1, where, when the scattering angle are equal to30 °and 45 °, the curves exhibit obvious oscillation, but when scattering angle was setting to 60 °, 75 °and 90 °, $F\sim D$ curves become smooth, and the larger the scattering angle, the smoother, which indicates that in this situation there are significant monotonic relationships between F and D.
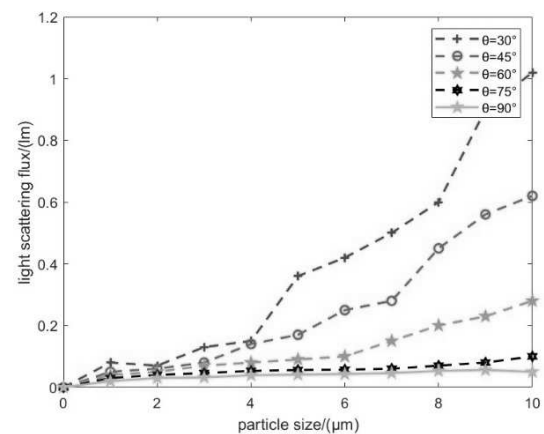

Fig. 1 *Simulation curve of light extraction direction angle and F~D characteristics*
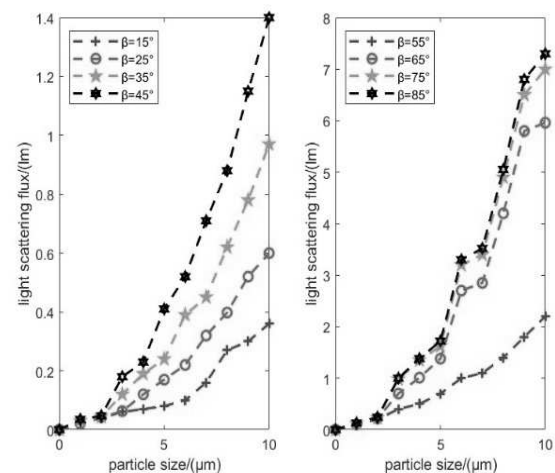

Fig. 2 *Simulation curve of light-harvesting stereo angle and F~D characteristics*

Similarly, by setting scattering angle (θ) at 90 °, the $F \sim D$ curves at different solid angle ($\Delta\Omega$ =15°, 25°, 35°, 45°, 55°, 65°, 75° and 85 respectively) could be obtained as shown in Fig. 2, where, no matter the values of $\Delta\Omega$, there always present fine coherence between F and D. But further information can also be drawn from Fig.2 that when $\Delta\Omega$ is in 55°~65° range, F is approximately linearly related to the square of the particle size (D^2) within several specific particle size ranges (will discuss it detailly in 3.1 section). As it is well known that for a photodetector, there is linear correlation between the input signals (light intensity of flux) and output signals (voltage) within its measurement range. So according to simulation results that in the condition of by setting θ =90 ° and $\Delta\Omega$ =60° respectively, the output voltage (u) of photodetector will be proportional to the square of the spherical particle size (D^2), which can be expressed by equation 2.

$$u = aD^2 + b \qquad (2)$$

$$C = \frac{M}{V} = \frac{N \times m}{V} = \frac{\pi}{6} \cdot \frac{N}{V} \cdot \rho \cdot D^3 \qquad (3)$$

Where:

u…The output voltage for the photodetector [V];
D…The particle size [m];
a and b…Constants;
m…The mass of the single particle [µg];
ρ…The density of spheric particle [µg·m⁻³].

For the aerosol sample composed of spherical particles with the same density and size, if PN is known, then its mass concentration can be calculated by equation 3, i.e., mass concentration (C) of the sample is directly proportional to the number of particles per unit volume (N/V), particle density (ρ), and particle size (D) which could be calculated from equation 2.

Therefore, as long as the relationship between D and u, particles number per unit volume and the particle density can be measured or accurately obtained, the particle mass concentration in each particle size channel can be calculated. And then, by accumulate the mass concentrations of each channel in less than 2.5µm or 10µm, PM$_{2.5}$ and PM$_{10}$ could finally be obtained.

2.1.2 Development of PM$_{2.5}$/PM$_{10}$ monitors

The schematic diagram of designed PM$_{2.5}$/PM$_{10}$ monitor is shown in Fig. 3, where sampling module, optical module (sensor based on light scattering), circuit module and software module are mainly involved. Sampling module should pump aerosol samples into the optical module of the monitor at a constant flow rate and minimize humidity interference on light scattering signals as much as possible. In view of this, a Dynamic Heating System (DAS) with 1m effective heating length was first designed. By continuously heating the pumped aerosol sample, the moisture attached on particles could be removed, thereby ensuring the reliability of particle sizing derived from light scattering flux. In DAS there mainly are humidity sensor for ambient aerosol, sampling inner tube with heating resistance wire wrapped externally and temperature sensor, temperature & humidity dynamic control circuit, and temperature insulation layer with outer-shell, etc. Base on the obtained humidity results obtained by the in-build sensor, on-off of heating resistance wire, temperature inside the sampling inner tube could be controlled automatically. Here, the heating function will not be activated in humidity less than 30%, while when humidity is in 30% -88%, and larger than 88%, the heating temperature are set at 40 °C and 60 °C separately.

A gas pump (Thomas G3/04) was used as the drawing source to let the aerosol sample into the monitor at nominal flow volume of 1L/min. More than that, a flow monitoring unit is built in flow circuit, by using it and PID algorithm, constant flow output of the gas pump can be achieved.
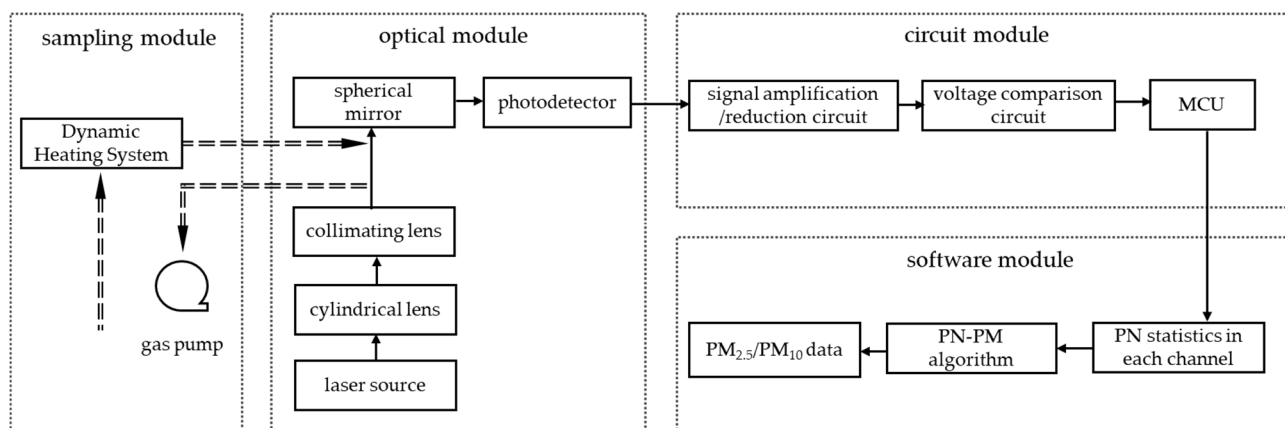

Fig. 3 *Schematic diagram of the structure of PM$_{2.5}$/PM$_{10}$ monitor*

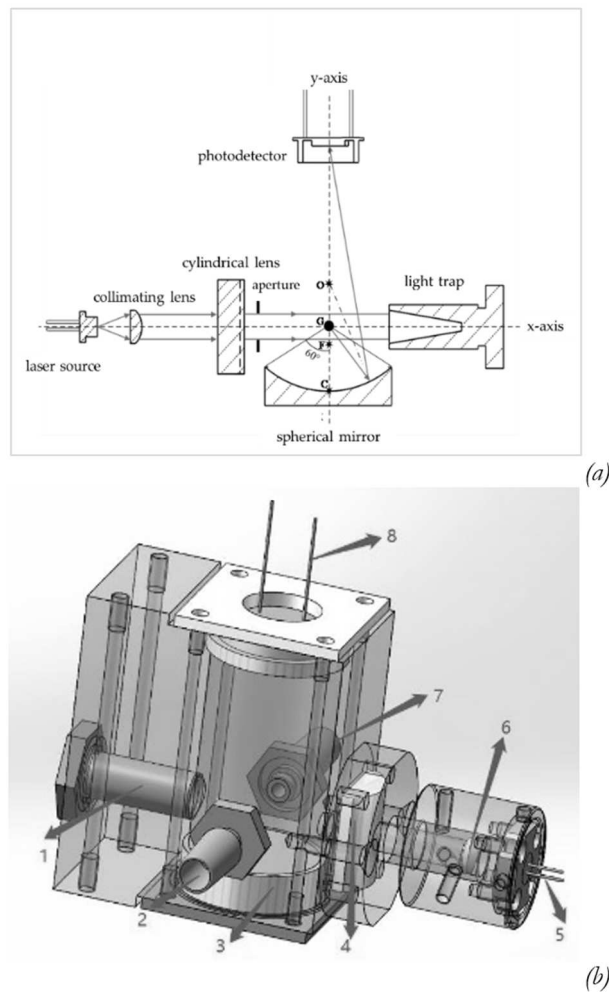*(a)*

(b)

Fig. 4 *Schematic diagram (a) and mechanical structure diagram (b) of the SPLSS*

Where:
1…Light trap，
2…Outlet，
3…Spherical mirror，
4…Cylindrical lens，
5…Laser source，
6…Collimating lens，
7…Inlet，
8…Photodetector.

As the key component of monitor and for achieving accurate results of $PM_{2.5}/PM_{10}$ concentration, optical module (sensor) should be of the measurement capability with upper limit not less than 10μm. Although the number concentration of particulate matter in the atmospheric air tends to increase with the decrease of particle size, particles less than 0.3μm have an ignored influence on $PM_{2.5}/PM_{10}$. So, considering of R&D costs, the particle size lower limit for monitor as low as 0.3μm is sufficient. Based on the simulation results described in 2.1 section, a kind of single particle light scattering sensors (SPLSS) with (0.3~10) μm measurement capability was

designed as shown in Fig. 4 (a), where, point C, O, and F are the vertices, curvature centers, and focal points of the spherical mirror, respectively, and point G is the particle position, also known as the photosensitive zone position.

This sensor is mainly composed of a laser source (with 650nm wavelength, 10mW power), collimating lens (with outer diameter Φ 6mm, radius of curvature R 4.15mm, focal length f 8mm), cylindrical lens (with radius of curvature R 10mm, focal length f 20mm), spherical mirror (with outer diameter Φ 25 mm, focal length f 10mm, radius of curvature R 20 mm), photodetector (with 6mm×6mm photosensitive area and 0.38 A·W⁻¹ photoelectric conversion efficiency), aerosol inlet/outlet and light trap, etc. The distances of the vertices of the spherical mirror to the center of the photosensitive region and to the photodiode are 11.6 mm and 34.4mm. The mechanical and physical diagram of the sensor are shown in Fig. 4 (b).

As it is well known, sensor's physical resolution for particle size is dependent on its structure and employed optical components, etc. But in addition to this, if increasing the number of particle size channels appropriately, the ability for recognizing particles can also be increased, and accordingly, the measurement accuracy for particle mass concentration could be improved. Therefore, in this paper, a circuit module based on threshold comparison was developed to divide sensor's particle size channels into 16 channels, which are 0.3μm, 0.4μm, 0.5μm, 0.6μm, 0.7μm, 0.8μm, 0.9μm, 1μm, 1.5μm, 2μm, 2.5μm, 3μm, 4μm, 5μm, 7μm and 10μm. Meanwhile, for observing the original pulse signal from photodetector and further calibrating voltage corresponding to particle size, a BNC interface for outputting original signal is reserved. For the software module, there are three parts according to its function, MCU main program, flow monitoring & adjustment program, and data collection & processing program. And among them, data collection & processing program can process data according to the PN-PM algorithm, simultaneously output and store PN concentration of each particle size channel, $PM_{2.5}/PM_{10}$ results.

PN-PM algorithm mentioned here is a calculate method to obtain the corresponding mass concentration from the PN concentration in each channel. For light scattering sensors, D in equation 3 should be the equivalent particle size of the channel. Due to light scattering is more sensitive to particle's volume and surface area, the particle size base on volume surface area (D_{32}), can be obtained by equation 4, is selected as the equivalent particle size of the channel.

$$D_{32} = \frac{3}{4} \frac{D_{n+1}{}^4 - D_n{}^4}{D_{n+1}{}^3 - D_n{}^3} \qquad (4)$$

Where:

D_n and D_{n+1} respectively are lower and upper particle size limits of the channel n.

Density is critical to obtain believable mass results according to PN-PM algorithm. Research shows that the effective density of particles in ambient is not only regions and time dependent [22, 23], but also it is size dependent. Generally, by using high resolution online and in situ measurement techniques, effective density of particles could be measured [22]. In this paper, empirical data of effective density drawn by summarizing literature were adopted [22-26], that is, within the range of (0.3-1.0) µm, (1.0-2.0) µm, (2.0-5.0) µm and (5.0-10.0) µm, the effective density values were set to 1.60 g·cm⁻³, 1.90 g·cm⁻³, 2.10 g·cm⁻³, and 2.26 g·cm⁻³.

3 Discussion of results

3.1 SPLSS calibration and monitor's performance verification

3.1.1 Calibration of SPLSS

According to the analysis mentioned before, for accurately measuring the $PM_{2.5}$ and PM_{10}, it is necessary to establish a relationship of particle size and voltage ($D{\sim}u$) of SPLSS, as well as the particle counting efficiency within each particle size channel. In this paper, a calibration device based on monodisperse sample generation and static mixing was developed, as shown in Fig. 5, where aerosol generation system, calibration chamber, and standard measurement equipment are involved.
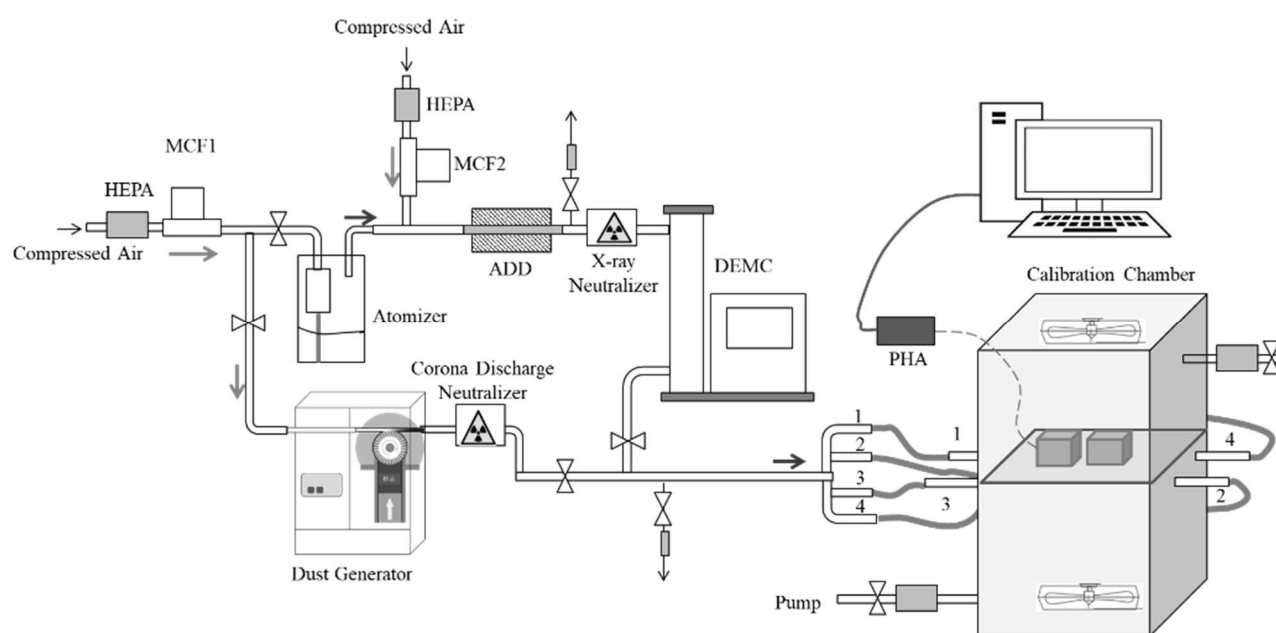

Fig. 5 *Schematic diagram of sensor calibration system*

Where:

MFC…Mass Flow Controller,

ADD…Aerosol Diffusion Drier,

PHA…Pulse Height Analyzer,

DEMC…Differential Electrical Mobility Classifier,

HEPA…High Efficiency Particulate air filter.

An atomizer and a dust generator available commercially are the main components of our aerosol generation system. Wherein, TOPAS ATM220 atomizer was used to atomize suspensions of polystyrene particle size reference material with different particle sizes, and after the droplets were passed through aerosol diffusion dryer, solid particles could be formed, and then after though aerosol neutralizer and Differential Mobility Classifier (TSI 3086), monodisperse aerosol sample with nominal size of (0.3~1.0) µm could be obtained. PALAS RPG1000 dust generator was used to generate monodisperse

powder polystyrene particles surface modified with sulfonic acid groups, and after this formed original aerosol sample passing though corona discharge neutralizer, monodisperse aerosol samples with nominal size of (1.0~10) µm, which are electrically neutral in total, could be obtained.

The design idea of the calibration chamber is as follows: 1) A rectangular cubic chamber with length, width and height of 75 cm, 75 cm and 100 cm respectively, where its internal volume is about 0.056m³; 2) Two fans with adjustable rotate speed were installed at the top and bottom of chamber, which can quickly improve the uniformity of aerosol samples inside the chamber; 3) A stainless steel support mesh was installed at its half height for placing calibrated sensors and reference instruments; 4) In the location of approximately 5cm above of the stainless steel support mesh, four aerosol inlets , with entrance section vertically upwards and 10cm away

from the edge of the chamber, were installed on both sides; 5) A draw outlet and an inlet were equipped on the top and bottom of the chamber for internal cleaning.

Uniformity of particle in the chamber, which is critical for obtaining reliable calibration data, is simulated by using Ansys Fluent software. As whole, the space of the chamber was firstly divided into 50mm grids. While in the region of aerosol inlets and fan blades, grids were subdivided into 1mm and 5mm. The solving model was set to Realizable k-e viscous model with an extensible Scalable Wall Function (SWF) and a discrete phase model, where, particles were set to spray along the normal direction for 10 seconds. The fan's blades were set to rotate around the Y-axis, with no translation speed in the 3-D directions. The boundary conditions were set as follows: the velocity of inlets was 0.5m·s⁻¹, the turbulence intensity and viscosity ratio were 5% and 10 respectively, and the wall surface outside the inlet were a standard roughness and non-slip stationary walls. during solving, mixed initialization was selected, time steps and time step size were 1000 and 1s, and the maximum number of iterations was 20.
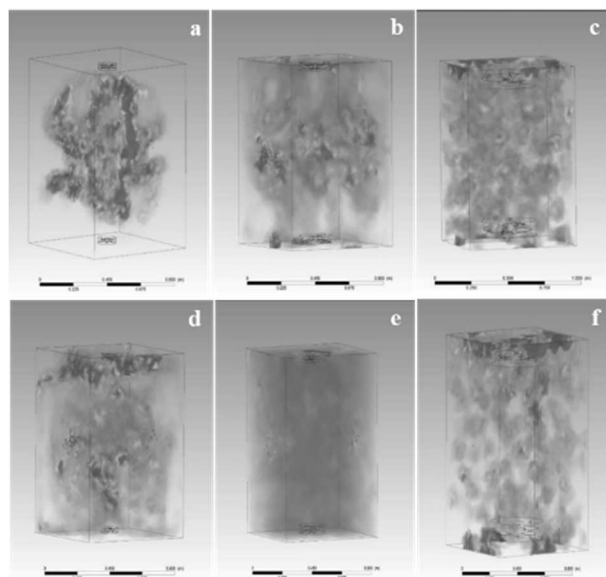

Fig. 6 *Mixing simulation diagram of calibration chamber*

Where:

a, b and c…Simulation results in the condition of using fans with different blade lengths (12cm, 20cm, and 30cm) and setting rotation speed to 50 r·min⁻¹.

d, e and f…Simulation results in the condition of using fans with blade lengths (12cm, 20cm, and 30cm) and setting rotation speed to 100 r·min⁻¹.

The simulation results were obtained as shown in Fig.6. By using fans with different blade lengths (12cm, 20cm, and 30cm) and setting rotation speed to 50 r·min⁻¹, the particles in the chamber exhibit disordered and non-uniformity states, as shown in Fig.

6 (a), (b), and (c). While in the condition of using fan with 20cm blade lengths and with 100 r·min⁻¹ rotation speed, the particles are evenly distributed in the chamber space, as shown in Fig. 6(e). Furthermore, under this operation condition, the uniformity of particle concentration in a square area with a side length of about 50cm (the shaded area in Fig. 7) above the support mesh section were tested. In this experiment, 0.5μm and 10μm polystyrene particles were generated successively, and particle number concentration larger than 0.3μm and larger than 5μm were measured respectively by using an optical particle counter (TSI 9306) at 9 different points in the area (as shown in Fig. 8). The final results are exhibited Fig.8, that the PN average values of ≥0.3μm and ≥5μm measured at 9 points in the concerned area are 23049 particles·L⁻¹ and 14894 particles·L⁻¹ respectively, with relative standard deviations of 2.2% and 3.3%.
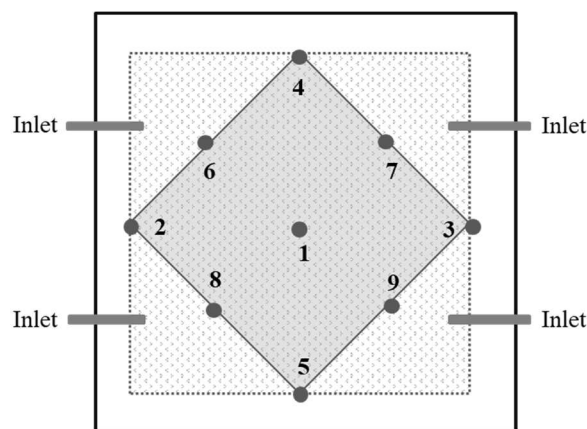

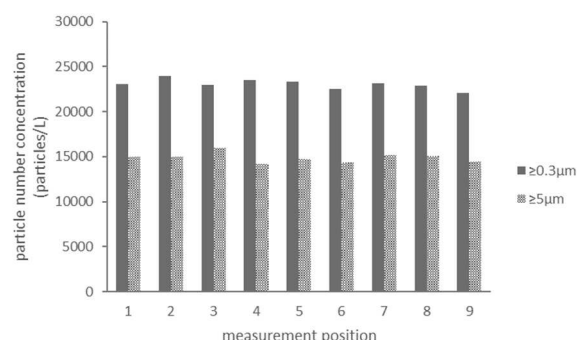**Fig. 7** *Schematic diagram of sampling location*

Fig. 8 *PN concentration in different sampling location*

When a kind of monodisperse aerosol sample was generated by using the calibration device and drawn into sensor, the mean pulse voltage derived from the particles passing through light scattering zone could be obtained by connecting pulse height analyzer (MCA-8000A) with signal output of sensor, which was the respondent voltage (u) to this particle size (D). So, in this way, the $u \sim D^2$ calibration curves in different particle size ranges could be finally established, As

shown in Fig. 9, the linearities (R^2) are 0.9724, 0.9974, and 0.9990 respectively in the range of (0.3-1) μm, (1-2.5) μm and (2.5-10) μm, which indicate the good linearity between u and D^2 for our designed SPLSS.
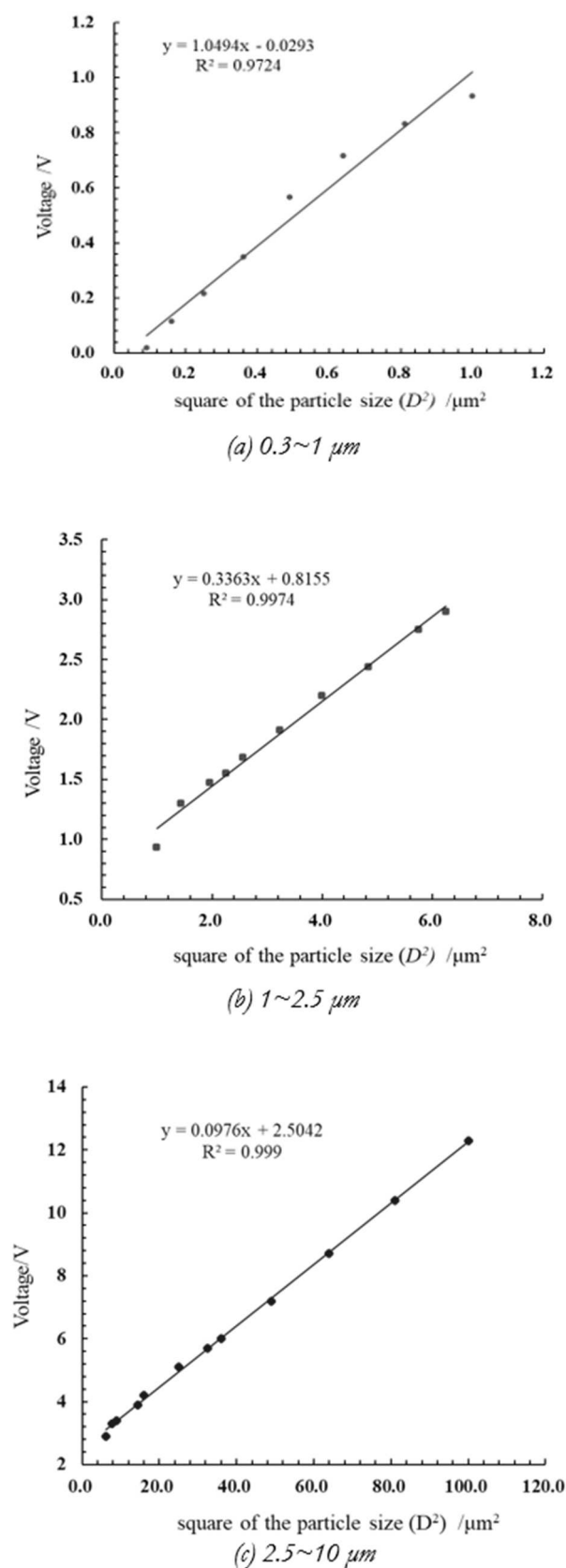

(a) 0.3~1 μm

(b) 1~2.5 μm

(c) 2.5~10 μm

Fig. 9 *Linear fit of u and D² in particle size range*

During particle counting efficiency calibration for SPLSS, the aerosol samples with nominal values of 0.3μm, 0.4μm, 0.5μm, 0.6μm, 0.7μm, 0.8μm, 0.9μm, 1.0μm, 1.5μm, 2μm, 2.5 μm, 3μm, 4μm, 5μm, 7μm and10μm were generated in order by using the above calibration system. By directly compared with reference particle counter (TSI9306), which have already been calibrated with condensation particle counter, particle counting efficiency in each channel of the sensor could finally be obtained. All calibrated results were exhibited in Fig. 10, where, within (0.3-10) μm range the particle counting efficiency of the sensor is in 93%~106%, error bars represent the calibration expanded uncertainty (k=2). Then those calibrated results were written into the software system of the monitor for correcting the particle counting value (N).
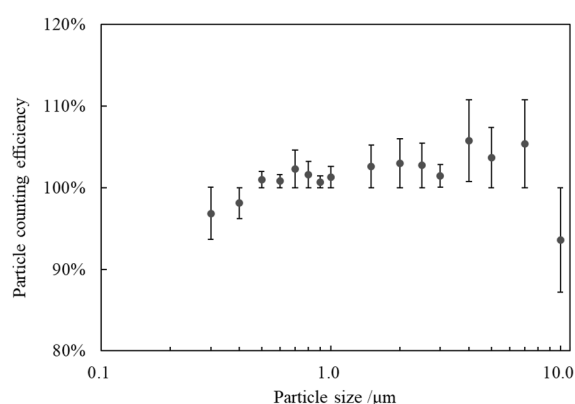

Fig. 10 *Calibration results of particle counting efficiency*

3.2 Performance verification of monitor

To verify the reliability of monitor for measuring $PM_{2.5}$ and PM_{10} in real environment, comparative tests were conducted with $PM_{2.5}$/PM_{10} samplers based on filter membrane weighing method in Chaoyang District, Beijing from April to May 2022. In this comparison period, the daily average of $PM_{2.5}$ and PM_{10} were in range of (5-130) μg·m^{-3} and (50-500) μg·m^{-3}. In comparison, for $PM_{2.5}$/PM_{10} samplers, sampling flow volumes are controlled within ± 3% of nominal flow volume (16.7L·min^{-1}). Fiberglass filter membranes was used to deposit atmospheric particulate matter. Before and after sampling, the blank and particle-deposited membranes were balanced for 24 hours in a constant Temperature & Humidity chamber, where T&H were controlled within (20 ± 0.2) ℃ and (50 ± 2) %RH, to eliminate the impact of moisture. And in the same T &H situation, masses of those membranes were weighted by using balance with resolution of 1μg. Finally, according to the mass difference of membrane deposited with particles after 24-hour-sampling and blank membrane and the sampling volume in standard

condition, the $PM_{2.5}$ or PM_{10} concentration could be calculated as standard values. For the monitor, the $PM_{2.5}$ or PM_{10} average values within 24 hours can be obtained by software. In this way, 15 pairs of $PM_{2.5}$ valid data pairs, and 16 pairs PM_{10} valid data pairs were obtained.

Fitting through linear regression of those data pairs, both $PM_{2.5}/PM_{10}$ results of developed monitor have good consistency with the filter membrane weighing method, as shown in Fig. 11. The parameters, i.e., slopes, intercepts, and correlation coefficients, in linear regression equation of $PM_{2.5}$ and PM_{10} results, meet the technical requirements of of Chinese standard (HJ653-2021), where, the specification of PM_{10} and $PM_{2.5}$ continuous automatic monitoring system including light scattering method are proposed.
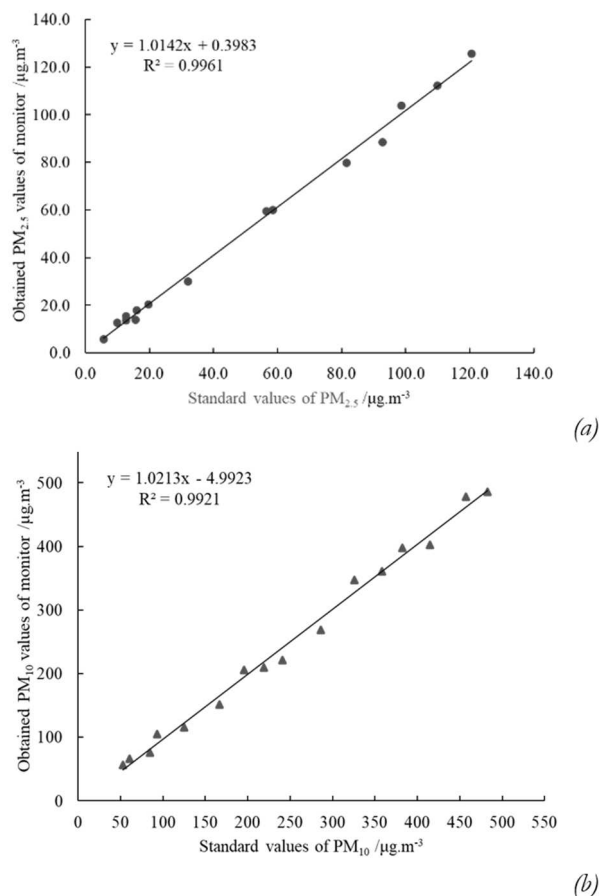

$$y = 1.0142x + 0.3983$$
$$R^2 = 0.9961$$

(a)

$$y = 1.0213x - 4.9923$$
$$R^2 = 0.9921$$

(b)

Fig. 11 *Comparison results of $PM_{2.5}$ (a) and PM_{10} (b) of monitor*

4 Conclusion

Low-cost $PM_{2.5}$ and PM_{10} monitoring instruments based on single particle light scattering was developed, which could measure $PM_{2.5}$ and PM_{10} in atmospheric air accurately. In this research, for precisely identifying the particle size, establish the quantitative relationship between the light scattering flux and the particle size is essential. While the simulation results show that in

the condition of scattering angle and the scattering solid angle are 90 ° and 60 ° respectively, within several specific particle size ranges the voltage signal of the photodetector has a good linear relationship with the square of the particle size. Based on this optimization result, the monitor's particle size range was divided into 16 channels using a threshold voltage comparison circuit. The calibration results indicate that the threshold voltage is linearly proportional to the square of particle size (D^2) within different particle size ranges, which is consistent with expectations.

For calibration and correction of the counting efficiency and particle size channel of SPLSS or monitor, a calibration device was developed, where, by using atomizer connected with differential mobility classifier and dust generator, monodisperse aerosol samples with peak value in (0.3~10) µm could be obtained. The simulation and experimental results indicate that the uniformity of particulate matter in the calibration chamber was fan blade length and rotate speed depend, and when the rotate speed was $100 r \cdot min^{-1}$ and the length of the fan blade was 20cm, the uniformity of the working section was better than 3.3%.

In the PN-PM algorithm, density is an important factor affecting the accuracy of calculated $PM_{2.5}$ and PM_{10} results. Although diversity of particle sources in aerosols, there is a certain correlation between particle composition and particle size. Therefore, the particle composition varies among different particle size segments, i.e., the density of particles within different particle size segments can be obtained from the density of their dominant particles. Bason on this consideration and referring to relevant research conclusions, in this paper, density values of particulate matter were set $1.60 \ g \cdot cm^{-3}$, $1.90 \ g \cdot cm^{-3}$, $2.10 \ g \cdot cm^{-3}$, and $2.26 \ g \cdot cm^{-3}$ within the range of of (0.3-1.0) µm, (1.0-2.0) µm, (2.0-5.0) µm and (5.0-10.0) µm. The feasibility of this kind of density-assignment method was verified through comparison with standard instruments. Certainly, due to the time limitations of the comparative experiment, the assigned density values in this paper still have the possibility of optimization.

References

[1] GARCIA, A., SANTA-HELENA, E., FALCO, A.N., RIBEIRO, J.P., GIODA, A.,

GIODA, C.R. (2023). Toxicological effects of fine particulate matter (PM$_{2.5}$): health risks and associated systemic injuries-systematic review. *Water Air Soil Pollut.*, Vol. 234, No. 6, pp. 346-369.

[2] BO, Y., BROOK, J.R., LIN, C., CHANG, L.Y., GUO, C., ZENG, Y., YU, Z., TAM, T., LAU, A.K.H., LAO, X.Q. (2021). Reduced ambient PM$_{2.5}$ was associated with a decreased risk of chronic kidney disease: A longitudinal cohort study. *Environ. Sci. Technol.*, Vol. 55, No. 10, pp. 6876-6883.

[3] FENG, S., GAO, D., LIAO, F., ZHOU, F., WANG, X. (2016). The health effects of ambient PM$_{2.5}$ and potential mechanisms. *Ecotoxicol Environ Saf.*, Vol. 128, No. 6, pp.67-74.

[4] ZHAI, S., JACOB, D.J., WANG, X., SHEN, L., LI, K., ZHANG, Y., GUI K., ZHAO, T. (2019). Fine particulate matter (PM$_{2.5}$) trends in China, 2013–2018: separating contributions from anthropogenic emissions and meteorology, *Atmos. Chem. Phys.* Vol. 19, No. 16, pp.11031-11041.

[5] LIU, G., DONG, X., KONG, Z., DONG, K. (2021). Does national air quality monitoring reduce local air pollution? The case of PM$_{2.5}$ for China. *J. Environ. Manage.*, Vol. 296, No. 4, 113232.

[6] SU, X.D., SUTARLIE, L., LOH, X.J. (2020). Sensors and analytical technologies for air quality: particulate matters and bioaerosols. *Chem-asian J.*, Vol. 15, No. 24, 4241-4255.

[7] LE, T., SHUKLA, K.K., CHEN, Y., CHANG, S., LIN, T., LI, Z., PUI, D.Y.H., TSAI, C. (2020). On the concentration differences between PM$_{2.5}$ FEM monitors and FRM samplers, *Atmos. Environ.*, 222, 117138.

[8] SHUKLA, K., AGGARWAL, S.G. (2021). Performance check of beta gauge method under high PM$_{2.5}$ mass loading and varying meteorological conditions in an urban atmosphere, *Atmos. Pollut. Res.*, Vol. 222, No. 4, 101215.

[9] GIORDANO, M.R., MALINGS, C., PANDIS, S.N., PRESTO, A.A., MCNEILL, V.F., WESTERVELT, D.M., BEEKMANN, M., SUBRAMANIAN, R. (2021). From low-cost sensor to high-quality data: A summary of challenges and best practices for effectively calibrating low-cost particulate matter mass sensors. *J. Aerosol Sci.*, Vol. 158, No.7, 105833.

[10] BARHATE, P.G., LE, T.C., SHUKLA, K.K., LIN., Z.Y., HSIEH, T.H., NGUYEN, T.T.N., LI, Z., PIU, D.Y.H., TSAI, C.J. (2022). Effect of aerosol sampling conditions on PM$_{2.5}$ sampling accuracy. *J. Aerosol Sci.*, Vol. 158, No. 7, 105968..

[11] GUPTA, P., DORAISWAMY, P., LEVY, R., PIKELNAYA, O., MAIBACH, J., FEENSTRA, B., POLIDORI, A., KIROS, F., MILLS, K.C. (2018). Impact of california fires on local and regional air quality: The role of a low-cost sensor network and satellite observations. *Geohealth*, Vol. 2, No. 6, pp.172–181.

[12] JAYARATNE, R., LIU, X., AHN, K., ASUMADU-SAKYI, A., FISHER, G., GAO, J., MABON, A., MAZAHERI, M., MULLINS, B., NYAKU, M., RISTOVSKI, Z., SCORGIE, Y., THAI, P., DUNBABIN, M., MORAWSKA, L. (2020). Low-cost PM$_{2.5}$ Sensors: An Assessment of their Suitability for Various Applications. *Aerosol Air Qual Res.*, Vol. 20, pp. 520-532.

[13] AIX M. L., SCHMITZ S., BICOUT D. J. (2023). Calibration methodology of low-cost sensors for high-quality monitoring of fine particulate matter. *Sci. Total Environ.*, Vol. 889, 164063.

[14] GUO, Q., ZHU, Z., CHENG, Z., XU, S., WANG, X., DUAN, Y. (2020). Correction of light scattering-based total suspended particulate measurements through machine learning, *Atmosphere*, Vol. 11, No. 2, pp. 139-156.

[15] CORDERO, J.M., BORGE, R., NARROS, A. (2018). Using statistical methods to carry out in field calibrations of low cost air quality sensors. *Sensors Actuat. B: Chem.* Vol. 267, pp. 245–254.

[16] FEENSTRA, B., PAPAPOSTOLOU, V., HASHEMINASSAB, S., ZHANG, H., BOGHOSSIAN, B.D., COCKER, D., POLIDORI, A. (2019). Performance evaluation of twelve low-cost PM$_{2.5}$ sensors at an ambient air monitoring site. *Atmos. Environ.*, Vol. 216, 116946.

[17] BI, J., CARMONA, N., BLANCO, M.N., GASSETT, A.J., SETO, E., SZPIRO, A.A., LARSON, T.V., SAMPSON, P. D., Kaufman, J. D., SHEPPARD, L. (2022). Publicly available low-cost sensor measurements for PM2.5 exposure modeling: Guidance for monitor deployment and data selection. *Environ. Int.*, Vol. 158, 106897.

[18] BI, J., WALLACE, L.A., SARNAT, J. A., LIU, Y. (2021). Characterizing outdoor infiltration and indoor contribution of PM$_{2.5}$ with citizen-based low-cost monitoring data, *Environ. Pollut.*, Vol. 276, 116763.

[19] SAYAHI, T., BUTTERFIELD, A., KELLY, K. E. (2019). Long-term field evaluation of the Plantower PMS low-cost particulate matter sensors. *Environ. Pollut.*, Vol. 245, pp. 932–940.

[20] TRYNER, J., L'ORANGE, C., MEHAFFY, J., MILLER-LIONBERG, D., HOFSTETTER, J.C., WILSON, A., VOLCKENS, J. (2020). Laboratory evaluation of low-cost PurpleAir PM monitors and in-field correction using co-located portable filter samplers. *Atmos. Environ.*, Vol. 220, 117067.

[21] WANG, Z., DELP, W., SINGER, B. C. (2020). Performance of low-cost indoor air quality monitors for PM$_{2.5}$ and PM$_{10}$ from residential sources. *Build. Environ.*, Vol. 171, 106654.

[22] PENG, L., LI, Z., ZHANG, G., BI, X.; HU, W., TANG, M., WANG, X., PENG, P., SHENG, G. (2021). A review of measurement techniques for aerosol effective density, *Sci. Total Environ.*, Vol.778, 146248.

[23] WU, T. Y., HORENDER, S., TANCEV, G., VASILATOU, K. (2022). Evaluation of aerosol-spectrometer based PM$_{2.5}$ and PM$_{10}$ mass concentration measurement using ambient-like model aerosols in the Laboratory. Measurement, Vol. 201, 111761.

[24] KHEBLI, A., AGUIB, S., NOUREDDINE, C., LALLIA, K., MOUNIR, M. (2021). Mathematical modeling and numerical simulation of the buckling stability behavior of hybrid beam. *Manufacturing Technology*, 21, 793-804.

[25] HU, M., PENG, J., SUN, K., YUE, D., GUO, S., WIEDENSOHLER, A., WU, Z. (2012). Estimation of size-resolved ambient particle density based on the measurement of aerosol number, mass, and chemical size distributions in the winter in Beijing. *Environ. Sci. Technol.*, Vol. 46, pp. 9941-9947.

[26] MAJKO, J., VAŠKO, M., HANDRIK, M., SÁGA, M. (2023). Challenges in Tensile Testing of Thermoplastic Composites Reinforced with Chopped Carbon Fibre Produced by Fused Filament Fabrication Method. *Manufacturing Technology*, 23, 216-24.